ELSEVIER

Journal of South American Earth Sciences 16 (2004) 743–758

Journal of
South American
Earth Sciences

www.elsevier.com/locate/jsames

Crustal structure of the Ribeira fold belt, SE Brazil, derived from receiver functions

George Sand França[a,b,*], Marcelo Assumpção[a]

[a]*Instituto de Astromomia, Geofísica e Ciências Atmosféricas, Universidade de São Paulo, SP 01060-970 CP 3386, Brazil*
[b]*Departamento de Física, Universidade Federal do Rio Grande do norte, natal, RN, 59072-970, C.P. 1641, Brazil*

Received 28 February 2003; accepted 31 December 2003

Abstract

Crustal thicknesses previously estimated by [J. Geophys. Res. 107 (2002) 2] in SE Brazil varied from 47 km in the middle of the Paraná basin to approximately 35 km in the Ribeira fold belt. We study the crustal structure of the Ribeira belt in more detail by identifying the Ps Moho converted phase and its multiple reflection PpPms, as well as using waveform modeling of receiver functions. We use phase-weighted slant stacking to identify the Ps and PpPms arrival times, which provides the v_P/v_S beneath each station. In inverting the receiver functions, we use average crustal velocities and initial models obtained from a deep seismic refraction line, as well as data from a timed quarry blast. The crustal thickness ranges 34–42 km with a thinning trend toward the coast. Crustal thickness correlates with elevation, indicating approximate regional Airy isostasy. Along the Serra do Mar coastal range, the average crustal Poisson ratio is about 0.25. The southern part of the Mantiqueira range has a higher Poisson ratio of 0.28. Stations near the São Francisco craton have a lower Poisson ratio of 0.23.

Keywords: Crustal thickness; Poisson's ratio; Receiver function

1. Introduction

Although, deep crustal structure is important for the understanding of regional tectonic evolution, the Brazilian shield is one of the least studied continental regions in the world, as shown by the compilation of deep refraction results by Christensen and Mooney (1995). In SE Brazil, only two deep refraction profiles have been carried out, both unreversed: in Itabira, Minas Gerais, showing a crustal thickness of approximately 42 km (Giese and Shutte, 1975), and in the Ribeira belt (Bassini, 1986). More recently, two complete deep refraction lines were shot in the Tocantins province in central Brazil (Perosi, 2000; Soares et al., 2001). These recent refraction experiments provide detailed information about crustal structure and a better understanding of the tectonic evolution of the Tocantins province, though they do not make up for the lack of information in other areas of Brazil.

However, analysis of teleseismic receiver functions (RF) can provide useful information about crustal structure, especially Moho depth, and have been extensively used in almost all continental areas. Despite some nonuniqueness problems in inverting RF traces (Ammon, 1990), the major features of the crustal seismic velocity profile, similar to the information obtained from deep refraction studies (Owens et al., 1987), can be estimated. When enough high-quality teleseismic events are recorded, RF studies give good estimates of v_P/v_S ratios (Zandt et al., 1995), Moho dip directions (Langston, 1977; Owens and Crosson, 1988; Zhang and Langston, 1995), and anisotropic layer identifications (McNamara and Owens, 1993; Peng and Humphreys, 1997; Levin and Park, 1997).

RF studies in SE Brazil started with the deployment of broadband temporary stations of the Brazilian Lithosphere Seismic Project. The first estimates of crustal thicknesses (Assumpção et al., 2002) showed thicker crust in the Paraná basin (average 44 km, with maximum 47 km) and relatively thinner crust in the São Francisco craton and adjacent Brasília belt (average 42 km), including parts of the Mantiqueira range. In the Paraná basin and the São Francisco craton, independent information on average crustal velocities were available, which enabled more accurate estimates. In the Ribeira belt, however, Assumpção et al. (2002) estimated crustal thicknesses without local data about the average crustal velocities and assumed standard

* Corresponding author.
E-mail address: george@dfte.ufrn.br (G.S. França).

0895-9811/$ - see front matter © 2004 Elsevier Ltd. All rights reserved.
doi:10.1016/j.jsames.2003.12.002

values of 1.73 for the v_P/v_S ratio and 6.5 km/s for the average P-wave velocity. Herein, we determine crustal thickness and velocity profiles using information from one seismic refraction line and determine v_P/v_S ratios directly from RF data.

In Fig. 1a, we present the structural trends of the mainly Neoproterozoic Ribeira fold belt, limited to the north by the Brasília belt, the São Francisco craton, and the Araçuaí belt. To the west, the belt is buried by the Phanerozoic Paraná basin. The predominantly ENE structural trend in the south and central part of the belt changes to a NS direction to the northeast, merging with the Araçuaí belt and roughly following the Atlantic coast (Fig. 1a). Two main structural zones can be observed: a northern zone, closer to the São Francisco craton and Brasília belt, dominated by tangential tectonics with subhorizontal thrusts and nappes;

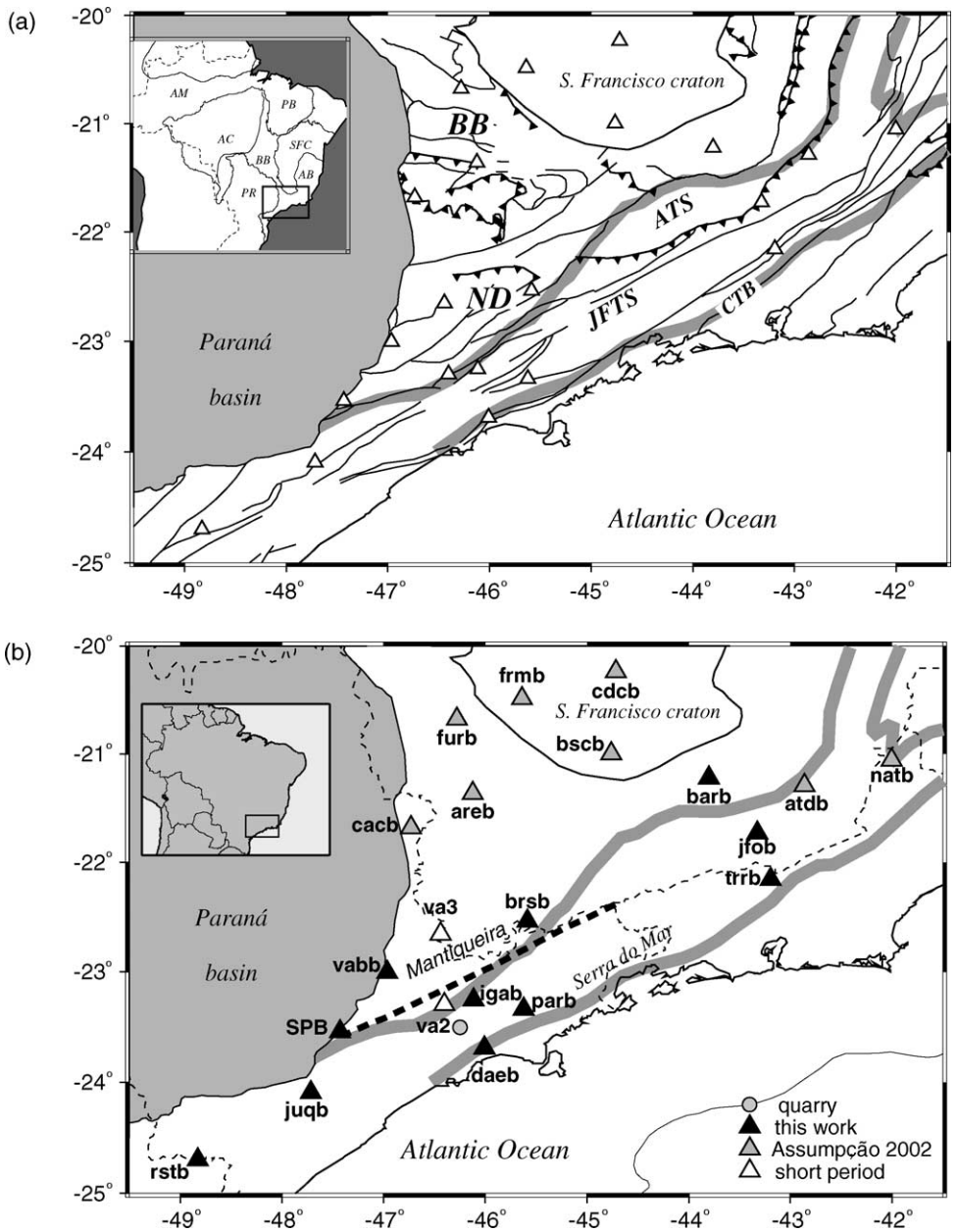

Fig. 1. (a) Location of the study area and main geological features of the Ribeira belt. ND, nappe domain in the transition zone south of the Brasília Belt (BB); ATS, Andrelândia thrust system; JFTS, Juiz de Fora thrust system; CTB, central tectonic boundary separating the Occidental from the Oriental terrane. Solid lines are transcurrent faults, and lines with teeth are thrust faults (Schobbenhaus and Bellizia, 2001). Triangles are seismic stations. In the inset, AB, Araçuaí belt; AC, Amazon craton; AM, Amazon basin; PB, Parnaíba basin; PR, Paraná basin; SFC, São Francisco craton. The thick gray lines show the limits of the main units of the Ribeira belts (Trouw et al., 2000; Heilbron and Machado, 2003). (b) Seismographic stations (triangles) and the Itapeti quarry (circle). Black triangles are broadband stations whose RF are analyzed herein; gray triangles are stations analyzed by Assumpção et al. (2002); white triangles are short period stations that recorded the Itapeti quarry blast. The thick dashed line is the seismic refraction profile (Bassini, 1986) of a quarry explosion near SPB. Thin dashed lines area state boundaries.

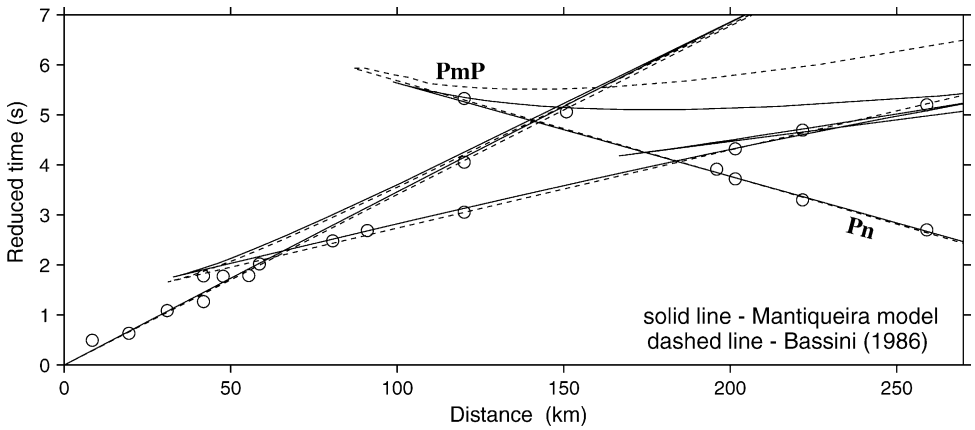

Fig. 2. P-wave travel time data (circles) from the refraction line of Bassini (1986) with his travel time curves shown as dashed lines. The same data were reinterpreted in this study (Mantiqueira model), and the travel time curves are shown as solid lines. Reduced time with reduction velocity of 7 km/s, X is distance. PmP is Moho reflection and Pn is upper mantle refraction.

and a southern zone closer to the Atlantic coast, dominated by transcurrent faults and vertical shear zones, mainly with dextral motion (Trompette, 2000). These long shear zones and the inflexion of the Ribeira belt around the São Francisco craton have been interpreted as the results of E–W convergence and escape tectonics related to the stiffer extremity of the São Francisco craton (Vauchez et al., 1994).

Trouw et al. (2000) and Heilbron and Machado (2003) divide the region into several tectonic-stratigraphic units. To the north, in the Mantiqueira range, a transition or interference zone is characterized by a nappe domain at the southern end of the Brasília belt (ND in Fig. 1a), and a foreland domain next to the São Francisco craton. Southeast of this interference zone, the Ribeira belt is composed of two main units, the Occidental and Oriental terranes, separated by a shear zone-the central tectonic boundary-developed during the later stages of the Brasiliano orogeny. The Occidental terrane includes the Andrelândia and the Juiz de Fora thrust systems (Trouw et al., 2000) and contains pre-1.8 Ga basement slivers interlayered with Neoproterozoic passive margin successions (Heilbron and Machado, 2003). The younger Oriental terrane first accreted to the São Francisco margin at ca. 580 Ma (Heilbron and Machado, 2003). The seismic stations for this work (Fig. 1b) cover the transition/interference zone between the Brasília and Ribeira belts (Brasília nappe domain) and the Occidental terrane (Juiz de Fora thrust system).

2. Average crustal velocities

2.1. Seismic refraction profile along Mantiqueira range

Bassini (1986), who estimated the crustal structure in the Ribeira belt with an unreversed seismic refraction line along the Mantiqueira range (Fig. 1b), used quarry blasts near station SPB (Fig. 1b). A cross-over approximately 60 km away (Fig. 2) marks a discontinuity at 8 km, between an upper crustal layer with $v_P = 5.8$ km/s, and a deeper layer with $v_P = 6.3$ km/s. Bassini (1986) interpreted all arrivals as refractions and used a single layer, from 8 km to the Moho discontinuity, to obtain a crustal thickness of 36.3 km. P-wave velocities in the continental lower crust tend to be higher than 6.6 km/s (Christensen and Mooney, 1995), though refractions from the lower crust are not always observed as first arrivals. Wide-angle reflections from the Moho discontinuity are often observed as large amplitude secondary arrivals in the 80–150 km distance range and can be used to constrain the lower crust velocities. Using a model with higher velocities in the lower crust, we reinterpret the arrival time data in Fig. 2 (Fig. 3); secondary arrivals at distances of 120–150 km are interpreted as

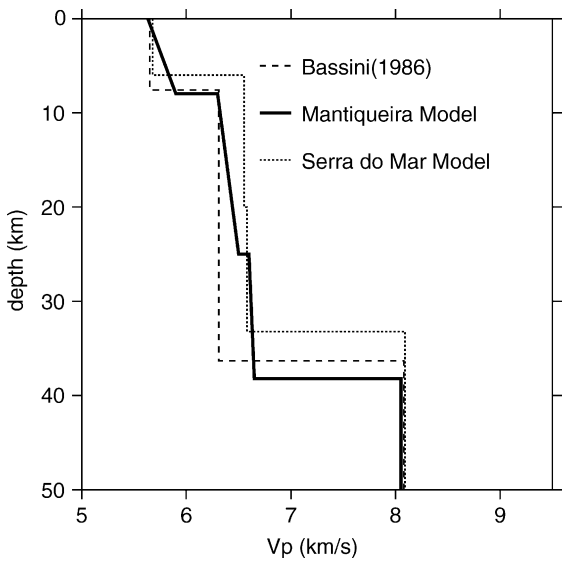

Fig. 3. P-wave velocity models; dashed line is Bassini's model of refraction line (Bassini, 1986); thick solid line is our re-interpretation of that refraction line (Mantiqueira model); thin solid line is the approximate model from a quarry explosion near DAEB (Serra do Mar model).

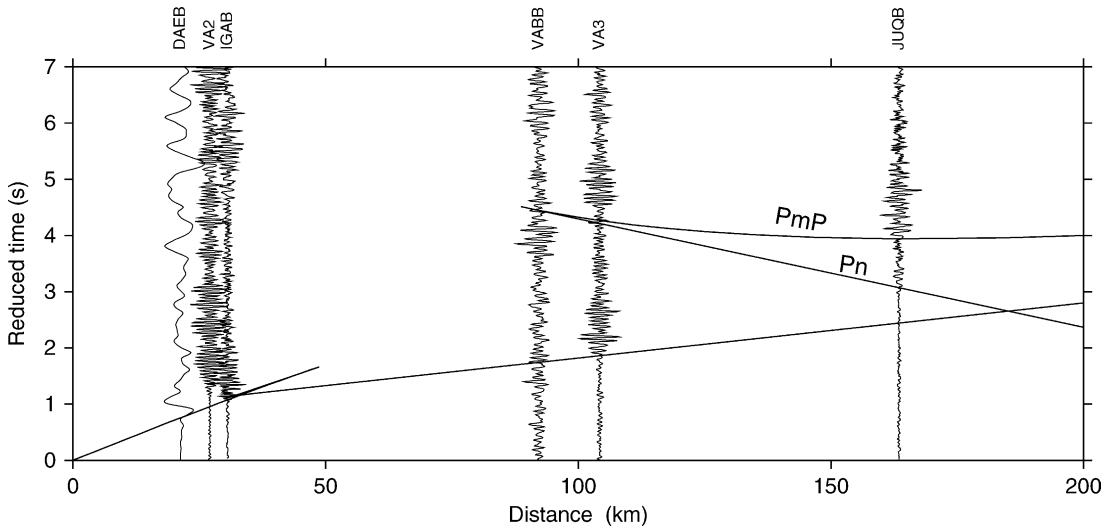

Fig. 4. P-wave seismic section from Itapeti quarry (normalized amplitudes) with travel time curve from Serra do Mar model in (Fig. 3). Reduced time with reduction velocity of 7 km/s, X distance. PmP is Moho reflection and Pn is upper mantle refraction. The DAEB trace has lower frequency content due to smaller sampling rate.

wide-angle reflections from the Moho, and secondary arrivals at 200–260 km are interpreted as wide-angle reflections from the top of the lower crust. We use velocity gradients to place the critical distances just before the observed reflected arrivals. Our estimate of the average crustal thickness therefore is 37.3 km. Because of the spacing of the stations, available arrival time data from the quarry blasts allow a range of possible models. However, our Mantiqueira model (Fig. 3) has an average crustal P-wave velocity of 6.48 km/s, in agreement with the average values ($v_P = 6.42 \pm 0.23$ km/s) compiled by Christensen and Mooney (1995) for continental shield areas.

2.2. Serra do Mar model

To constrain average crustal velocities in the Serra do Mar coastal range, we timed a 15-ton Itepeti quarry explosion recorded at stations DAEB, IGAB, JUQB, VA2, VA3 and VABB (Figs. 1 and 4). Because the stations are not aligned along a single profile, more scatter from lateral variation is expected in the record section; therefore, only a first-order average model is possible. First arrivals at up to 30 km (DAEB, VA2, and IGAB) show velocities similar to the Mantiqueira model, though the first arrival to station VA3 indicates slightly higher velocities for the mid-crustal layer. Secondary arrivals at VA3 and JUQB are interpreted as Moho reflections (PmP). The upper mantle refraction (Pn) and Moho reflection (PmP) at JUQB suggest a crustal thickness of 33 km and average crustal P-wave velocity of 6.4 km/s, as shown in Fig. 3. Thinner crust along the Serra do Mar range (Itapeti quarry-JUQB), compared with the Mantiqueira model, is consistent with the expected crustal thinning towards the coast. Although, insufficient data are available for a well constrained crustal model, the crustal average P-wave velocity of 6.4 km/s is useful for estimates of crustal thicknesses from RF.

In addition to a first-order P-wave velocity model, the Itapeti quarry data provided information about average v_P/v_S ratios along the coast. Table 1 shows the travel time ratios of the clear arrivals. The nearby stations show that v_P/v_S ratios in the upper crust are below the standard 1.73 value, whereas the Moho reflected waves indicate larger average v_P/v_S for the whole crust. If the upper crust has an average v_P/v_S ratio of 1.68, the lower crust should have v_P/v_S ratio approximately 1.80.

3. Receiver functions

RFs are waveforms computed by deconvolving the vertical component from the radial or tangential component, by which process the effects of the source and the instruments are eliminated They are a response of the structure beneath the station (Langston, 1979; Owens et al., 1984; Ammon, 1991), in which the teleseismic P-wave, incident on interfaces with S-wave contrasts, generates P to S converted waves. An example of RF is shown in Fig. 3, which assumes lateral homogeneity and plane wave incident at the bottom of the layer. The converted S-waves are

Table 1
Estimates of average v_P/v_S between the Itapeti quarry and stations based on S- and P-wave travel time ratios

Station	Distance (km)	t_S/t_P	Phases
DAEB	21.2	1.68	Upper crust refraction Sg/Pg
IGAB	30.6	1.68	Upper crust refraction Sg/Pg
VA3	104.2	1.78	Moho reflection SmS/PmP
JUQB	169.3	1.74	Moho reflection SmS/PmP

labeled according to the number of reverberations. We use Ps and PpPms waves because they are more easily recorded than later phases.

In Fig. 1, we provide the locations of the broadband stations used in this work. Assumpção et al. (2002) give preliminary estimates of crustal thickness for BARB, BRSB, IGAB, PARB and TRRB, and we reestimate those stations with more data. The RF was computed with routines supplied by Charles J. Ammon. To reduce the instabilities in the deconvolution due to spectral holes in the vertical component, we use a water level method (Clayton and Wiggins, 1976; Owens et al., 1984, 1987) with values chosen for each event of 0.001–0.01. We apply a low-pass gauss filter [$\exp(-\omega^2/4a^2)$] to reduce high frequency noise and scattering from small-scale heterogeneities. The gauss filter width a was set to 2 or 4, as a low-pass filter with corner frequency at ~1 or 2 Hz in RF, respectively. The time windows for the P-wave train were different for each observation; we selected the best window, usually 30–80 s, with the lowest noise in the RF trace (Fig. 5).

The RF were stacked for different ranges of distance and azimuth to improve signal-to-noise ratio. The stacked RF for IGAB and JUQB with Gaussian parameters 2 and 4 appear in Fig. 6. The radial component is shown by a solid line, the transverse by a dashed line, and the number of traces in parenthesis. The arrows mark the observed time of Ps Moho converted phase. The transverse component indicates the degree of lateral variability; no transverse component would be observed if there were only horizontal

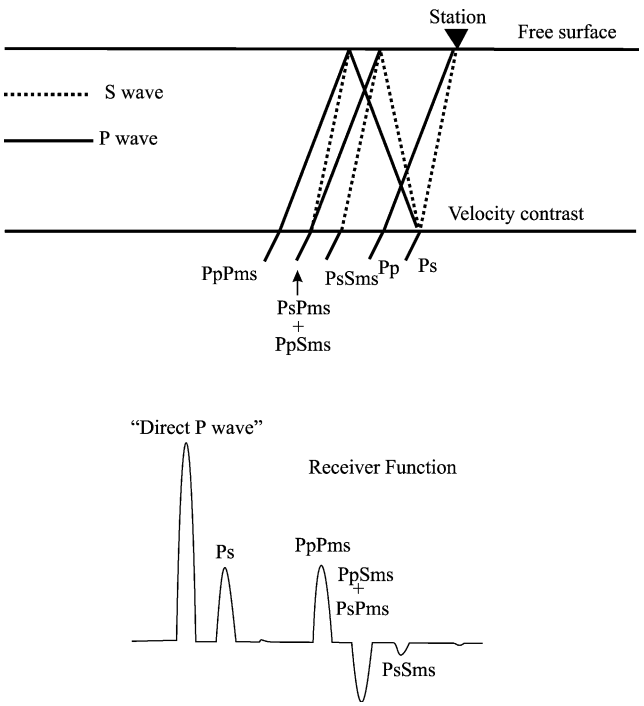

Fig. 5. Ray diagram of RF. (top) Simplified ray diagram showing the largest reflections and reverberations of the converted S phases, which make up the radial RF for one layer over a half-space. (bottom) RF seismogram corresponding to the reflections of the top diagram (Ammon, 1991).

layers beneath the station. In this study, however, we are interested only in the radial component.

The stacks show a clear Ps conversion phase for all stations. The PpPms phase is very clear at IGAB station. The time difference Ps–P decreases with increasing epicentral distance (decreasing incidence angle of the P wave at the Moho), whereas PpPms shows the opposite. Some RFs were determined for distances less than 30°, at which some influence from mantle triplication might be expected. However, because the number of events between 30° and 90° is not large, we include information from the closer distances.

A summary of the RF for all stations is shown in Fig. 7, where all traces were stacked (after correction of the Ps move out) to enhance the Moho converted Ps phase. Stations in Serra do Mar have shorter Ps–P times compared with other sites, indicating thinner crust.

3.1. Ps and PpPms identification

The Ps converted phase arrives about 5 s after the direct wave in continental stable areas and usually is identified easily (Fig. 6), whereas the PpPms phase is not always easy to identify in the seismograms. The PpPms phase has a larger offset (distance between the incidence point at the Moho and the station) than the Ps phase (Fig. 5) and therefore is more affected by lateral variations, scattering, and inelastic attenuation.

To identify the multiple phase PpPms, we stack all the seismograms. Due to the move out of the Ps and PpPms waves, slant stacking is necessary. The direction of stacking is varied to cover the expected move outs of the Ps and later phases. The Ps–P and PpPms–P times, however, do not vary linearly with the epicentral distance, as shown in Fig. 8a. Slant stacking with the epicentral distance would introduce misalignment errors, particularly at distances of less than 30°, as in Fig. 8a and b. To improve the linearity of the Ps–P (and PpPms–P) times between traces, we substitute the epicentral distance with the square of the slowness (Fig. 8c and d). This substitution is justified because the move out depends on the square of the slowness. Thus, the Ps–P times are more linearly related, and misalignment errors should be less than 0.01 s, including traces at close distances. The slope of the Ps–P times in Fig. 8c is 0.0046 s/(s/deg)^2, and the line fitting the PpPms–P is -0.015 deg^2/s.

We perform a test of the slant stacking technique with synthetic RF calculated with two different theoretical models (Fig. 9) composed of several 2-km thick layers and constant $v_P/v_S = 1.73$. The 'gradient', model has an average crustal P-wave velocity of 6.5 km/s with no large mid-crust discontinuity and a Moho depth of 36 km. Model 'LVZ' has an average P-wave velocity of 6.3 km/s, a mid-crustal low-velocity zone, and a Moho depth of 30 km. We generated synthetic RF for epicentral distances (and slowness) similar to those observed at station IGAB (Fig. 6).

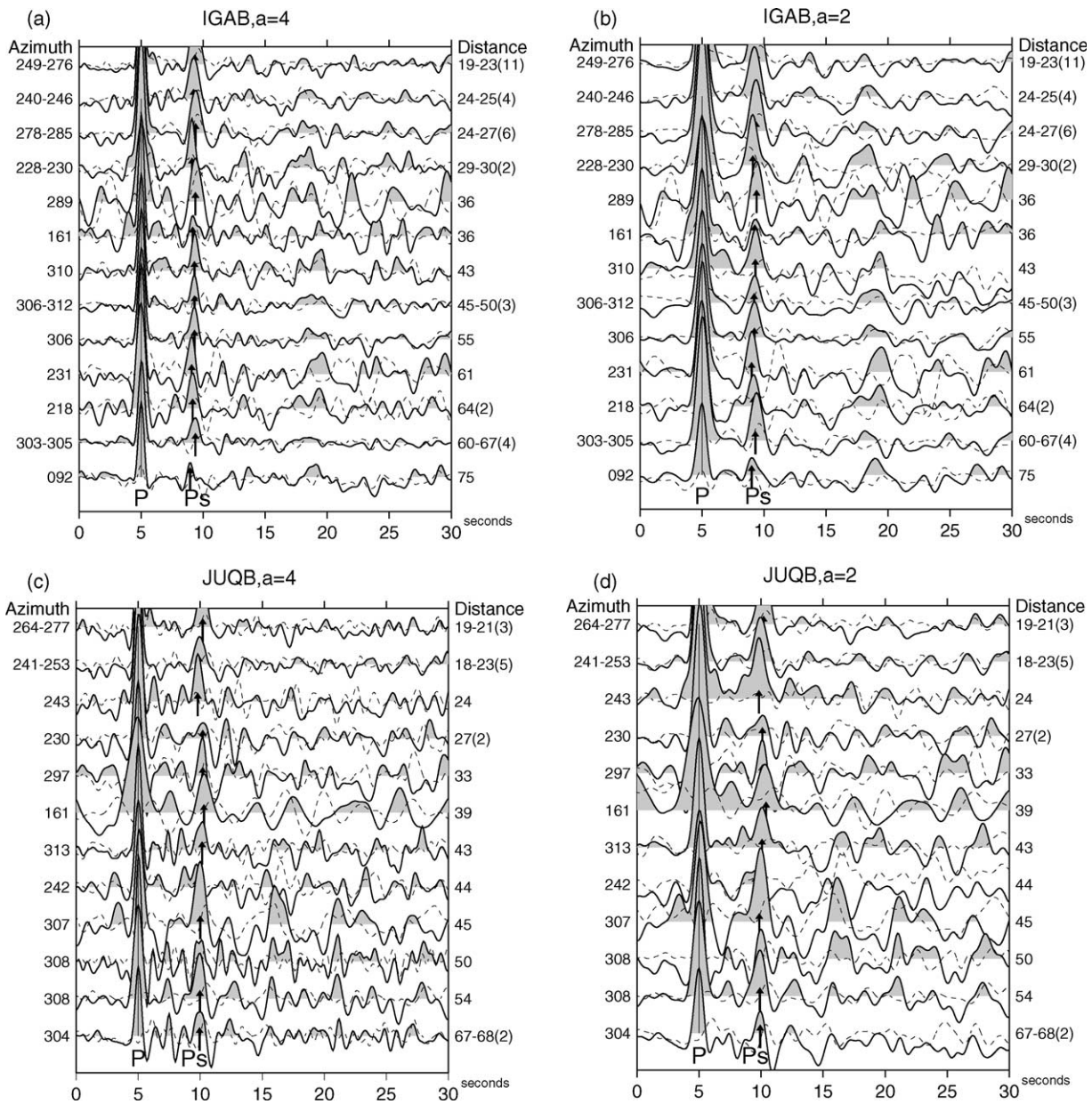

Fig. 6. Examples of RF for various azimuth and distance bins. Solid and dashed lines are radial and transverse components, respectively. The arrows mark the observed time of Moho Ps conversion. Numbers on the left are the azimuth ranges (measured at the station) of the events used in each stack; numbers on the right are the distance range with number of traces used in the stack shown in parentheses. The stacks are ordered by average slowness. Gauss filter width $a = 2$ and 4. For the IGAB station a clear PpPms arrival can be seen 15 s after the direct P.

The synthetic traces have Ps arrivals near 10 s, the multiple PpPms near 20 s and PsPms + PpSms of approximately 23 s with a negative peak (Fig. 10). Real data (Fig. 6) do not show the multiple PpPms as clearly, and the PsPms + PpSms arrivals are buried by noise.

We use the trace at 47° (slowness = 7.68 s/deg) as the reference trace; all other RF are slant stacked to the reference trace using slopes in the range -0.05 to $+0.05$ deg^2/s. Fig. 11 shows the contour of the stacked amplitudes (only positive amplitudes are plotted) normalized to amplitude 1 at the direct peak (time = 5 s, slope = 0). Gray contours are shown for amplitudes of 0.1–0.8 in steps of 0.01. The Ps and the PpPms peaks are shown with the contour line (thick solid line) for the 90% amplitude of each peak. We attempt both linear stacking (LS) and phase-weighted stacking (PWS). The Ps peak appears at 9.2 s and slope $+0.005$ deg^2/s; and the PpPms at 19.2 s and slope -0.015 deg^2/s. The peak slope values agree with the line fitting of the travel times shown in Fig. 8, as expected.

In addition to LS (simple sum of the amplitudes in each trace), we employ PWS (Schimmel and Paulssen, 1997), which uses signal coherency between traces as weights in the sum. Coherency is based on the instantaneous phase of the analytical signal. When the phases of all traces are

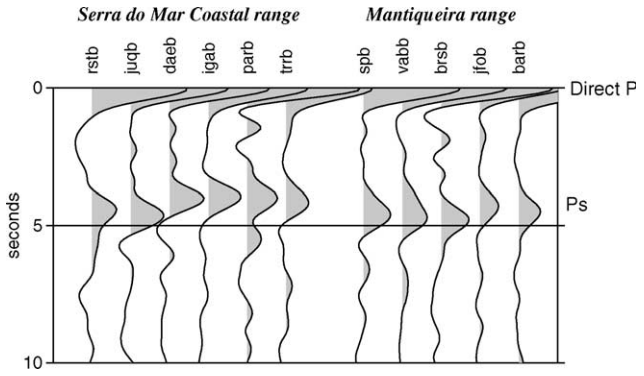

Fig. 7. Cross-section of stacked RF. For each station, all traces were stacked after move-out correction of the Ps phase to simulate vertical incidence. The stations in the Serra do Mar coastal region have shorter Ps–P times, on average, than the Mantiqueira group.

the same at a particular point, the weight is maximum (1.0). When phases are different among the traces, the amplitude of the LS is reduced, and PWS permits the detection of weak but coherent arrivals. More details about PWS methodology are explained by Schimmel and Paulssen (1997).

The synthetic test in Fig. 11 shows that the Ps and PpPms peaks have higher amplitudes (compared with the normalized peak of the direct P) and are sharper in PWS than in LS. Thus, PWS provides a more accurate picking of the Ps and PpPms times.

3.2. Average crustal v_P/v_S ratio

Picking the Ps and PpPms arrival times relative to the direct *P* enables the determination of the average crustal v_P/v_S ratio For an equivalent one-layer crustal model, v_P/v_S can be estimated as follows (Zandt et al., 1995)

$$\frac{v_P}{v_s} = \sqrt{(1 - p^2\bar{v}_P^2)\left[\frac{2(t_{Ps} - t_P)}{t_{PpPms} - t_{Ps}} + 1\right]^2 + p^2\bar{v}_p^2}, \quad (1)$$

where p is the reference ray parameter (slowness) and $\bar{v}_P$ is average crustal P-wave velocity. Zandt et al. (1995) show that the estimate of the average v_P/v_S is not too sensitive to the average crustal P-wave velocity ($\bar{v}_P$). In the theoretical model, $v_P/v_S = 1.73$. The errors in the estimated v_P/v_S ratio

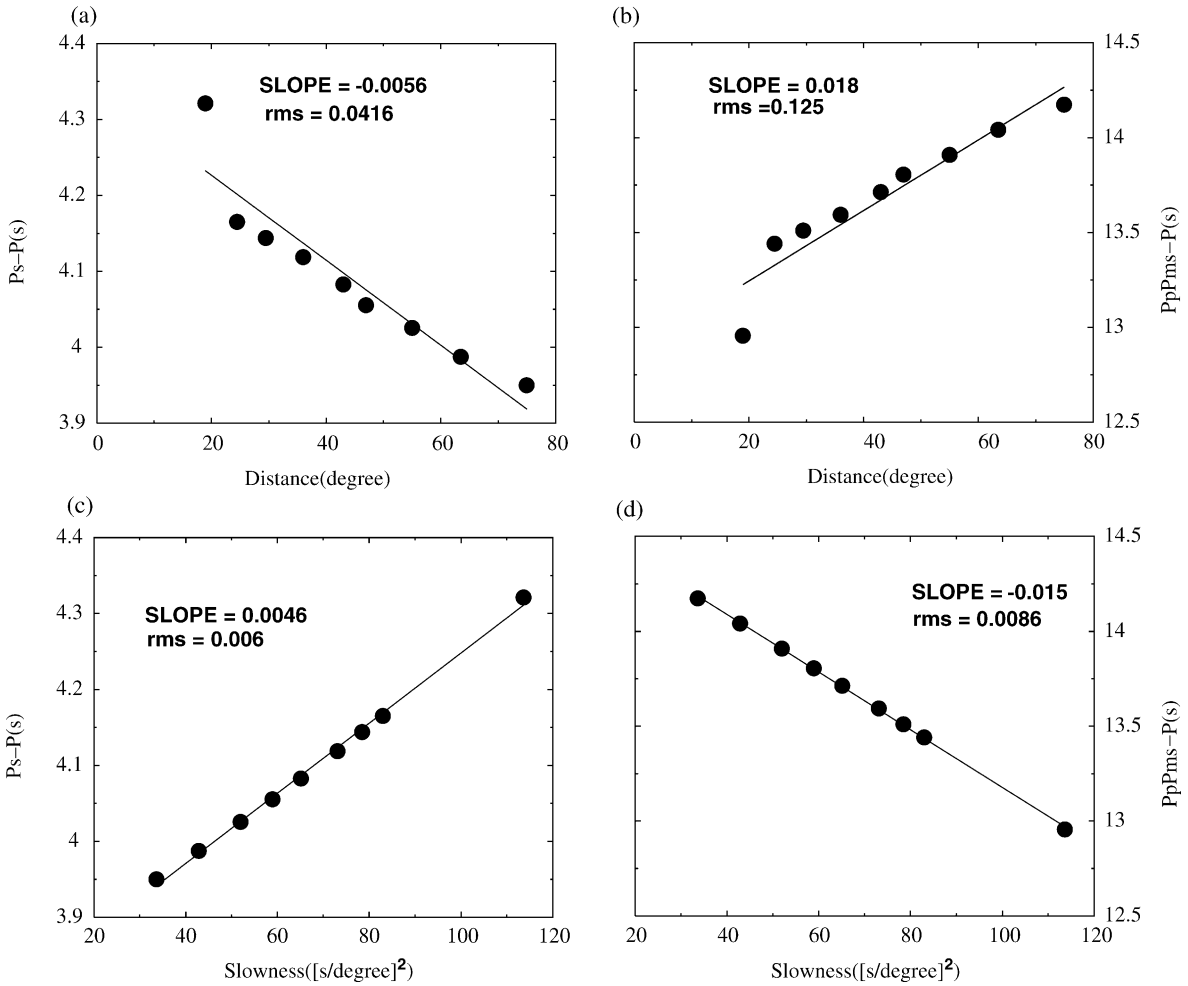

Fig. 8. Variation of the differential times Ps–P and PpPms–P with distance and square of slowness. Data calculated with the iasp91 model for surface earthquake depth.

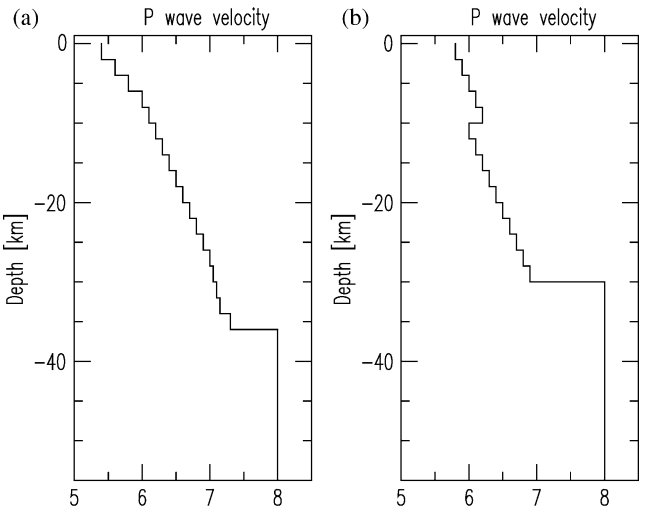

Fig. 9. P-wave velocity models used in the synthetic test. (a) Gradient model with average *P* velocity 6.5 km/s and Moho depth 36 km. (b) LVZ model with average *P* velocity 6.3 km/s and Moho depth 30 km.

using the slant PWS method with the gradient model were ~0.002 for $a = 4$, ~0.01 for $a = 2$, and ~0.04 for $a = 1$ (Table 2). The LVZ model gives similar results. The larger error for $a = 1$ (low pass corner frequency ~0.5 Hz) is due to the larger width of the Ps and PpPms pulses which cause more interference with neighboring pulses and thus shifts in the maxim locations. High gauss filter parameter values (greater than four) produce sharper peaks with more accurate time picks; however, higher frequencies make the traces more susceptible to scattering by small-scale crustal irregularities. A good compromise was found with gauss filter parameters of 2 or 4. In Figs. 12 and 13, we provide the slant PWS results for all analyzed stations in the Ribeira belt, using gauss parameter $a = 2$.

After determining the Ps and PpPms arrival time with the slant PWS, we calculated the velocity ratio v_P/v_S for each station (Table 3). We used two different crustal models for the average P-wave velocity. For the coast stations, based on Serra do Mar model, we used 6.4 km/s; for the more inland stations, based on the Mantiqueira model, we used 6.5 km/s. By knowing the v_P/v_S ratio (slant PWS diagrams) and the average P-wave crustal velocity (Serra do Mar or Mantiqueira models), we can determine the crustal thickness under each station (Zandt et al., 1995)

$$h = \frac{t_{Ps} - t_P}{[(v_s^{-2} - p^2)^{1/2} - (v_p^{-2} - p^2)^{1/2}]}. \quad (2)$$

For each station, we use Eq. (2) for all stacked traces. For example, for station IGAB, we calculated the Moho depth for 13 Ps–P times (Fig. 6). The average and standard deviations of these 13 measurements are shown in Table 3. The standard deviations indicate the degree of lateral variation in the crust beneath the station and do not include uncertainties in the v_P/v_S ratio or average crustal P-wave velocity.

Table 3 shows v_P/v_S and crustal thickness for the stations we analyzed in the Ribeira belt. The average value for the Serra do Mar coastal range, $v_P/v_S = 1.74$, is in good agreement with that obtained for the Itapeti quarry-JUQB path (Table 1). The IGAB and DAEB stations provide similar results for Moho depth and velocity ratio. The large v_P/v_S for the station PARB may be due to the few available traces with good RF (only four traces were used because of short operation time). If we use the Ps-P time with $v_P/v_S = 1.73$ for station PARB, we obtain the same 35 km thickness as the other two stations. We, therefore, conclude that the coastal region near these three stations has a crustal thickness of approximately 35 km and v_P/v_S ratio ≈1.72–1.73. The upper crust near DAEB and IGAB has $v_P/v_S = 1.68$ (Table 1); the lower crust must have higher v_P/v_S, probably around 1.76–1.78. This variation may reflect

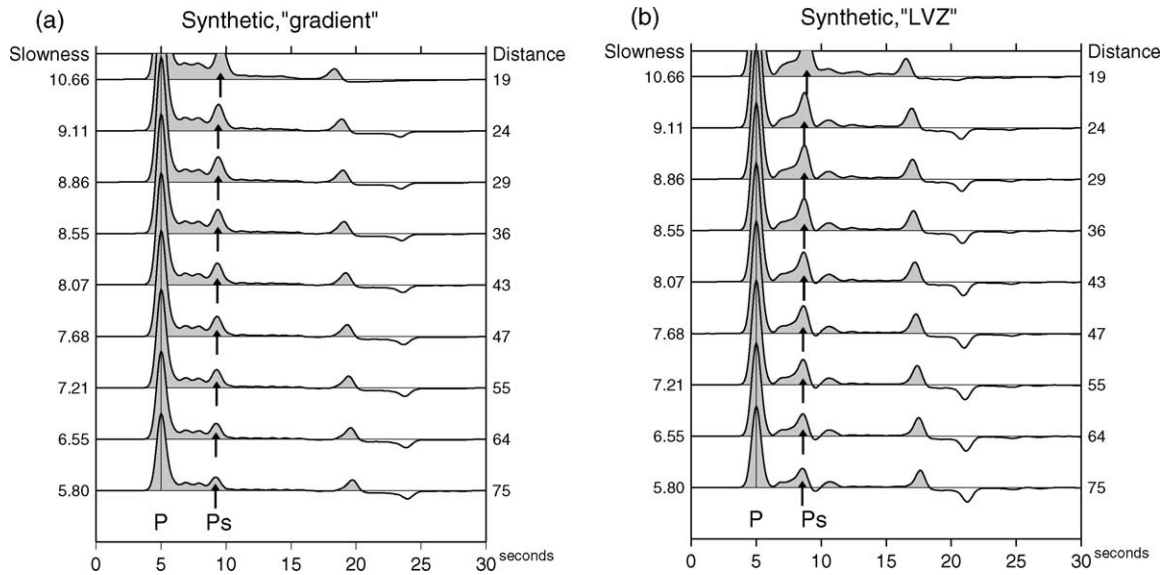

Fig. 10. Synthetic RF for various slownesses (or distances) used to test the PWS. Gauss parameter $a = 2$.

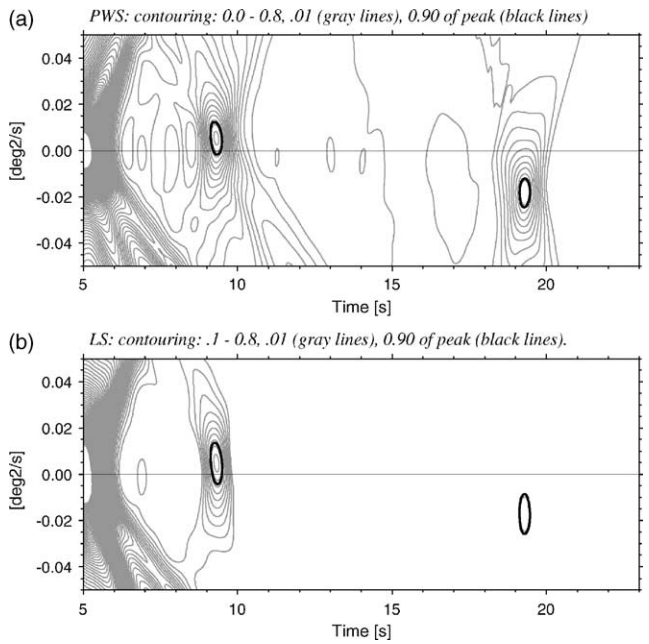

Fig. 11. Amplitude contour for PWS (top) and LS (bottom) using the synthetic seismograms from Fig. 10a (gradient model) and a reference slowness of 7.68 s/deg (distance of 47°). The gray lines are amplitude contours in steps of 0.1, with the direct *P* at 5 s normalized to 1. The black solid lines represent the contours with 90% amplitude of the peaks for Ps and PpPms phases.

a change of predominantly felsic rocks in the upper crust (e.g. granites and granodiorites, with Poisson ratio around 0.25) to more mafic rocks in the lower crust (e.g. gabbro with Poisson ratio around 0.29), according to Christensen (1996). In the platform and shield regions, the average v_P/v_S ratios for the whole crust compiled by Christensen (1996), Holbrook et al. (1992), and Zandt and Ammon (1995) range 1.76–1.86. Our results for the Serra do Mar range are lower (1.74, excluding the less reliable value of PARB) than those worldwide platform averages.

The crustal thicknesses of the three Mantiqueira stations—SPB, VABB, and BRSB—are 37–38 km, in good agreement with our re-interpretation of the nearby Mantiqueira refraction line (37.3 km; Fig. 3). These three stations also show consistently higher v_P/v_S ratio (1.80–1.85) than the Serra do Mar stations, which may indicate a more mafic average crustal composition for the lower crust in the Mantiqueira range. These three stations with high v_P/v_S ratios are in the same transition zone of the Brasília belt nappe domain (Fig. 1a). All other stations in the Occidental terrane, especially those in the Juiz de Fora thrust system, have consistently lower ratios (1.71–1.77).

Station BARB and JFOB were included in the Mantiqueira group because their average crustal velocity was taken from the Mantiqueira seismic refraction model. The low v_P/v_S ratios (BARB 1.66, JFOB 1.71) are consistent with the value of 1.70 obtained by Assumpção et al. (2002) in the São Francisco craton and adjacent belts.

Fig. 14 shows the calculated crustal thicknesses on a map of Bouguer anomalies. In general, lower Bouguer anomalies correspond to thicker crust. The crustal thickness of the coastal stations range 35–39 km and are smaller than those

Table 2
Results of v_P/v_S with slant stacking for two synthetic models with $v_P/v_S = 1.73$

Model	Gradient	LVZ
$\bar{v}_P$ (km/s)	6.5	6.3
h (km)	36	30
For $\alpha = 1$	$v_P/v_S = 1.694$	$v_P/v_S = 1.667$
For $\alpha = 2$	$v_P/v_S = 1.721$	$v_P/v_S = 1.715$
For $\alpha = 4$	$v_P/v_S = 1.728$	$v_P/v_S = 1.731$

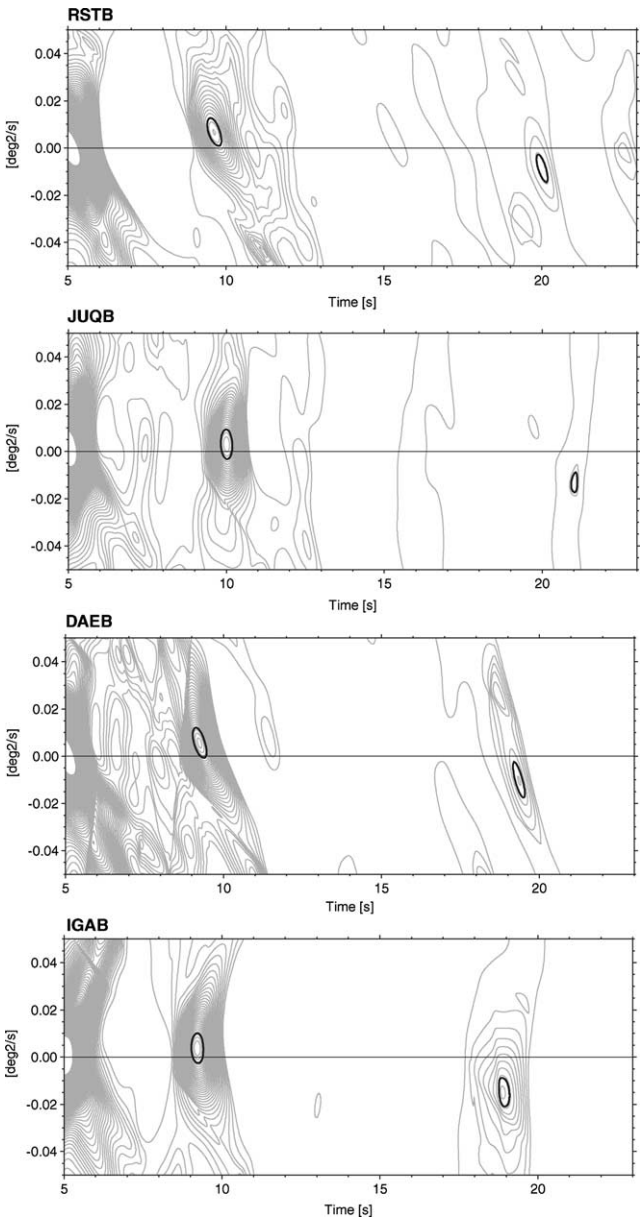

Fig. 12. Amplitude contour for PWS using real data for stations in Serra do Mar area (gauss parameter $a = 2$). The solid lines represent maximum coherence peaks for Ps and PpPms phases.

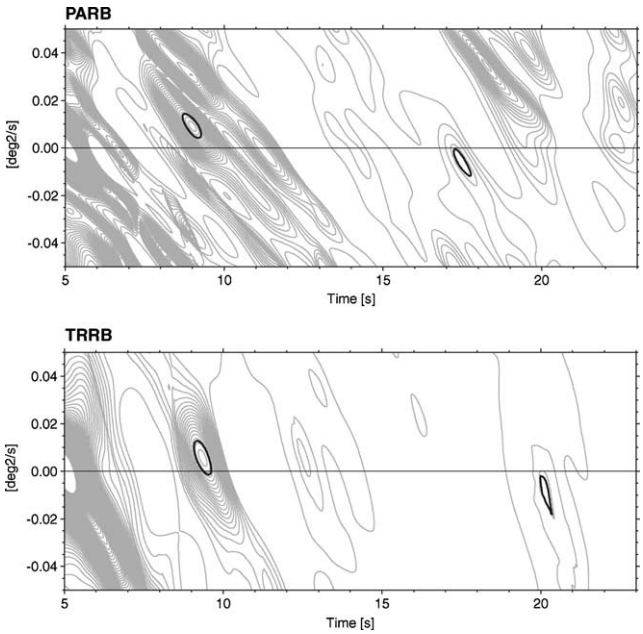

Fig. 12 (*continued*)

of stations farther from the coast (37–42 km). This difference is probably due to crustal thinning from the Atlantic rifting process. Stations with higher elevation tend to have lower Bouguer anomalies (Fig. 15a) and thicker crust, on average (Fig. 15b), as isostasy would predict.

4. Modeling RF

We calculated representative synthetic RF for each station to show the correct identification of the Ps and PpPms phases. Due to the non-uniqueness of RF inversions (Ammon et al., 1990) and the probable presence of scattered phases in the RF traces, we fit only the main features using simple, plain layer models. Our objective is to show that the estimates of crustal thickness and v_P/v_S are consistent with the observed RF.

We use the inversion procedure of Ammon et al. (1990), which consists of a linear iterative, least squares waveform fitting. An initial S-wave velocity model is taken to start the iterative inversions of matrix systems, which represent the minimization of the L2 norm of the misfit residual vector between the observed and modeled RF. Smoothness constraints are applied to minimize the second difference of the model parameters (S-wave velocity in each layer). To compute the RF for a given velocity structure, we use a technique based on propagator matrix method (Kennett, 1983). The P-wave velocities are adjusted with the v_P/v_S ratio, and the densities are adjusted with the relationship $\rho = 0.32v_P + 0.77$ (Berteussen, 1977).

For the initial models, we use the thickness and velocity ratio determined with the gauss parameter 2 (Table 3). Each model has a four-layer crust with average P-wave velocity

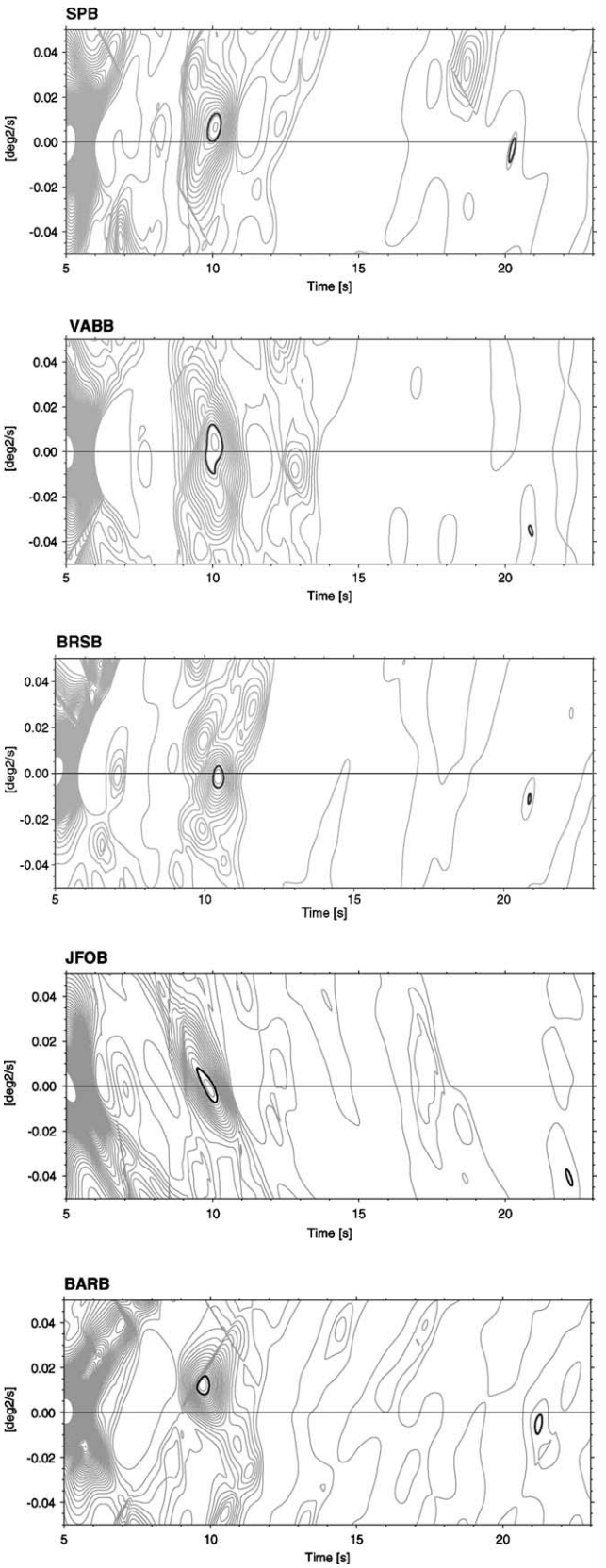

Fig. 13. Amplitude contour for PWS using real data for stations in Mantiqueira (gauss parameter $a = 2$). The solid lines represent maximum coherence peaks for Ps and PpPms phases.

Table 3
Values of v_P/v_S and crustal thicknesses (h) determined with RF using $\bar{v}_P = 6.4$ km/s for Serra do Mar coastal range and $\bar{v}_P = 6.5$ km/s for the Mantiqueira

	$a = 2$			$a = 4$			
	v_P/v_S	h (km)	$(Ps-P)_0$	v_P/v_S	h (km)	$(Ps-P)_0$	Elevation (km)
Serra do Mar coastal range							
DAEB	1.72	35.2 ± 1.0	3.99 ± 0.12	1.72	35.4 ± 0.8	4.00 ± 0.21	0.78
IGAB	1.74	34.2 ± 0.8	3.95 ± 0.10	1.72	34.9 ± 1.0	3.95 ± 0.12	0.68
JUQB	1.76	38.9 ± 1.6	4.62 ± 0.19	1.77	38.5 ± 1.5	4.66 ± 0.18	0.48
PARB	1.83?	31? ± 1.7	4.02 ± 0.23	1.85?	31? ± 2.0	4.11 ± 0.26	0.77
RSTB	1.77	36.7 ± 1.7	4.41 ± 0.21	1.75	37.4 ± 2.0	4.42 ± 0.24	0.17
TRRB	1.73	35.9 ± 2.3	4.11 ± 0.27	1.74	36.6 ± 2.5	4.14 ± 0.30	0.22
Mantiqueira range							
BARB	1.66	42.4 ± 2.8	4.34 ± 0.28	1.65	43.8 ± 2.1	4.37 ± 0.21	1.14
BRSB	1.85	36.9 ± 2.3	4.85 ± 0.30	1.80	39.8 ± 2.1	4.94 ± 0.26	1.85
JFOB	1.71	41.4 ± 2.8	4.52 ± 0.31	1.72	41.2 ± 3.1	4.56 ± 0.34	0.78
SPB	1.80	37.0 ± 2.3	4.56 ± 0.27	1.83	37.9 ± 2.3	4.67 ± 0.29	0.65
VABB	1.82	37.3 ± 2.7	4.68 ± 0.34	1.81	38.3 ± 3.1	4.79 ± 0.33	0.81

$(Ps-P)_0$ is the extrapolated Ps–P time for vertical incident; a, gauss parameter.

of 6.4 and 6.5 km/s for Serra do Mar and Mantiqueira stations, respectively. The smoothness constraint limits the rms residual to approximately the rms amplitude of the presignal noise (Ammon et al., 1990).

The modeling procedure for station IGAB appears in Fig. 16, with three RF with good signal-to-noise ratios from Fig. 6. The synthetic traces for the initial model (left column) fit the Ps and PpPms phases as expected, but they also fit the multiple PpSms + PsPms, which confirms that the crustal thickness and v_P/v_S ratio were estimated correctly. The final model differs little from the initial model for this station. In Figs. 17 and 18, we provide models Serra do Mar and Mantiqueira, respectively. The synthetic RF calculated with these simple models generally fit the multiple phases well, especially the Serra do Mar stations.

5. Discussion and conclusions

A problem in studying crustal structure with RF is the lack of independent information to constrain crustal thickness estimates. In our case, only one regional seismic refraction line was available in Mantiqueira (Bassini, 1986), the reinterpretation of which provides an average value for

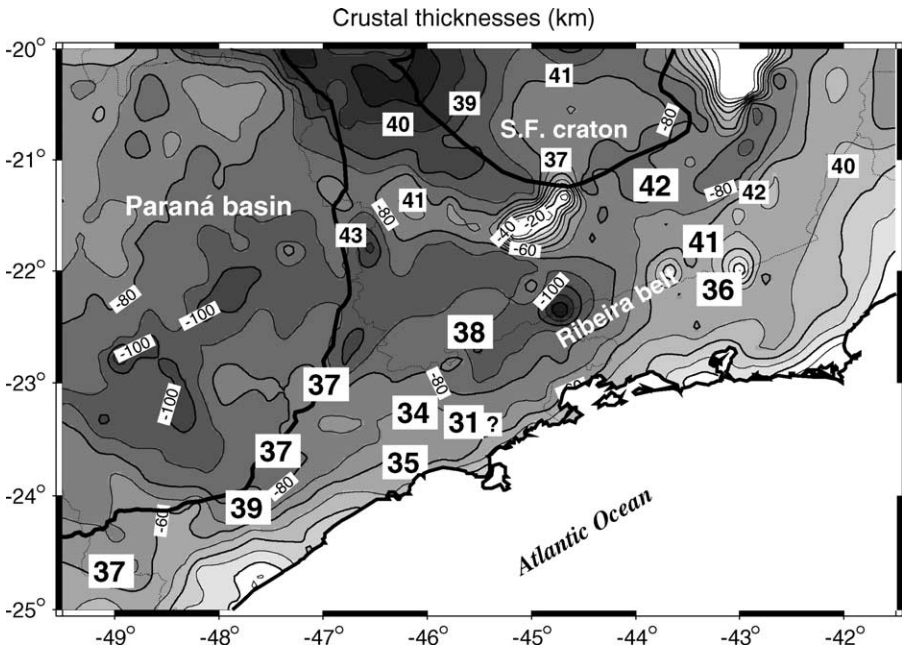

Fig. 14. Values of crustal thickness estimated using RF. Large numbers refer to stations analyzed herein (Table 3); small numbers are crustal thickness from Assumpção et al. (2002); Contours show Bouguer anomalies (IAG-USP database).

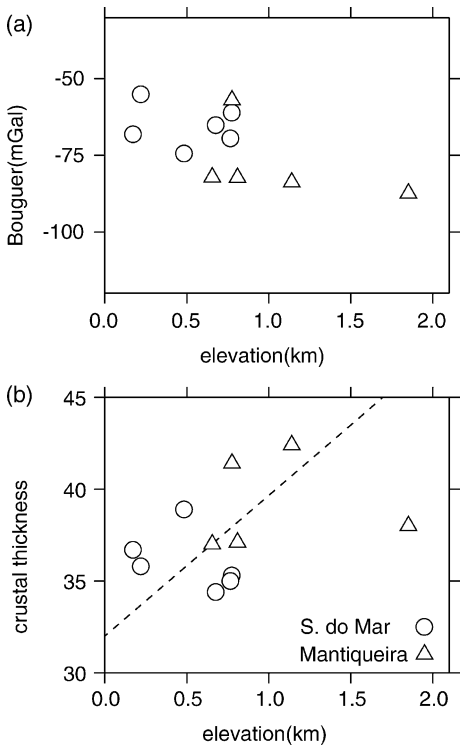

Fig. 15. (a) Variation of Bouguer anomalies with station elevation. (b) Variation of crustal thickness with station elevation. The dashed line is the expected relation from Airy isostasy, assuming a reference crustal thickness of 32 km for zero elevation and a 0.4 g/cm^3 contrast between lower crust and upper mantle.

the crustal P-wave velocity (6.5 km/s). Additional data from a quarry explosion indicate the average velocities in the Serra do Mar area (6.4 km/s).

We estimate crustal thickness using the RF time differences Ps–P and PpPms–P. Usually, the PpPms arrival has a poor signal-to-noise ratio. Using the slant PWS technique, we can identify this multiple phase and provide reliable values of the crustal velocity ratios.

The Serra do Mar coastal region has an average crustal thickness of 35 km and a reliably determined velocity ratio of 1.74. For some stations (DAEB and IGAB), the upper crust has a more felsic ratio (1.68), which suggests intermediate to mafic composition for the lower crust ($v_P/v_S \approx 1.78 - 1.80$). Away from the coast, the Mantiqueira stations have thicker crust (37–42 km), and those in southern Ribeira belt seem to have higher v_P/v_S ratios (1.80–1.85). Although, these velocity ratios are not as reliable as those for Serra do Mar (the PWS peak for the multiple PpPms is not as clear, Fig. 13), the results are consistent for the three stations, which are all located in the same geological unit (nappe domain) between the Brasília and the Ribeira belts (Fig. 1a). If these values are correct, the crust beneath SPB, VABB and BRSB has a more mafic average composition than the other sites. The low v_P/v_S ratio at the BARB and JFOB stations is comparable to the values found by Assumpção et al. (2002) near the San Francisco craton.

Stations in the Serra do Mar have lower elevations and thinner crust, on average, than more inland stations.

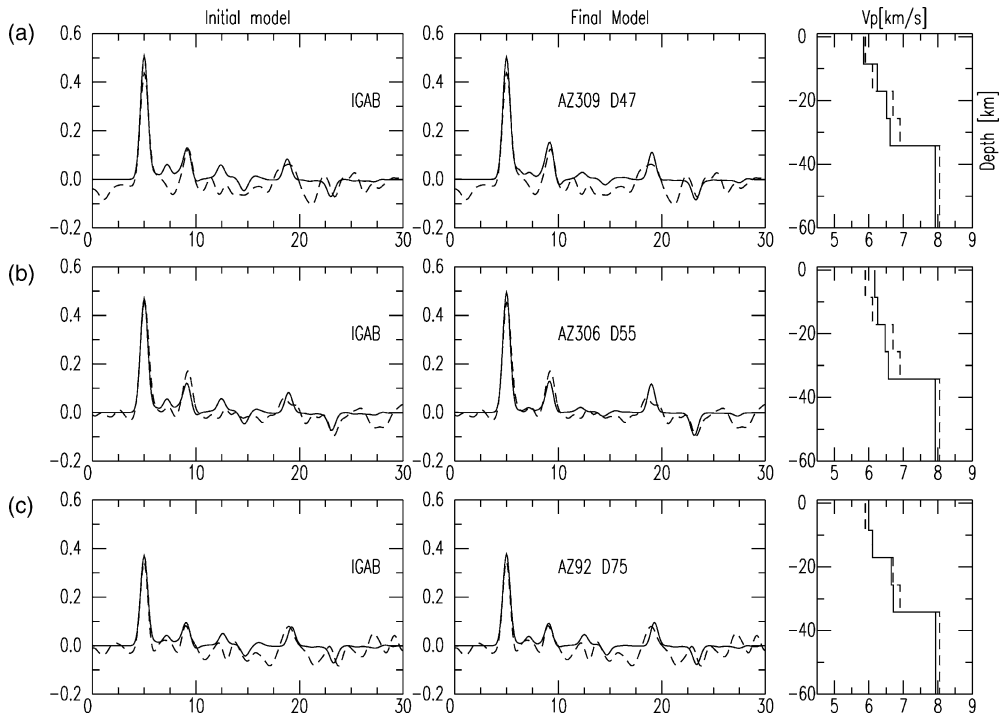

Fig. 16. Examples of synthetic RF for three stacked traces for station IGAB. Left-hand column shows the observed trace (dashed line) and the synthetic trace calculated with the initial model (solid line). Center column shows the inverted RF (solid line) with a slightly better fit; the labels indicate the azimuth and distance of the observed trace. Right-hand column shows the initial crustal model (dashed line) and the final inverted model (solid line).

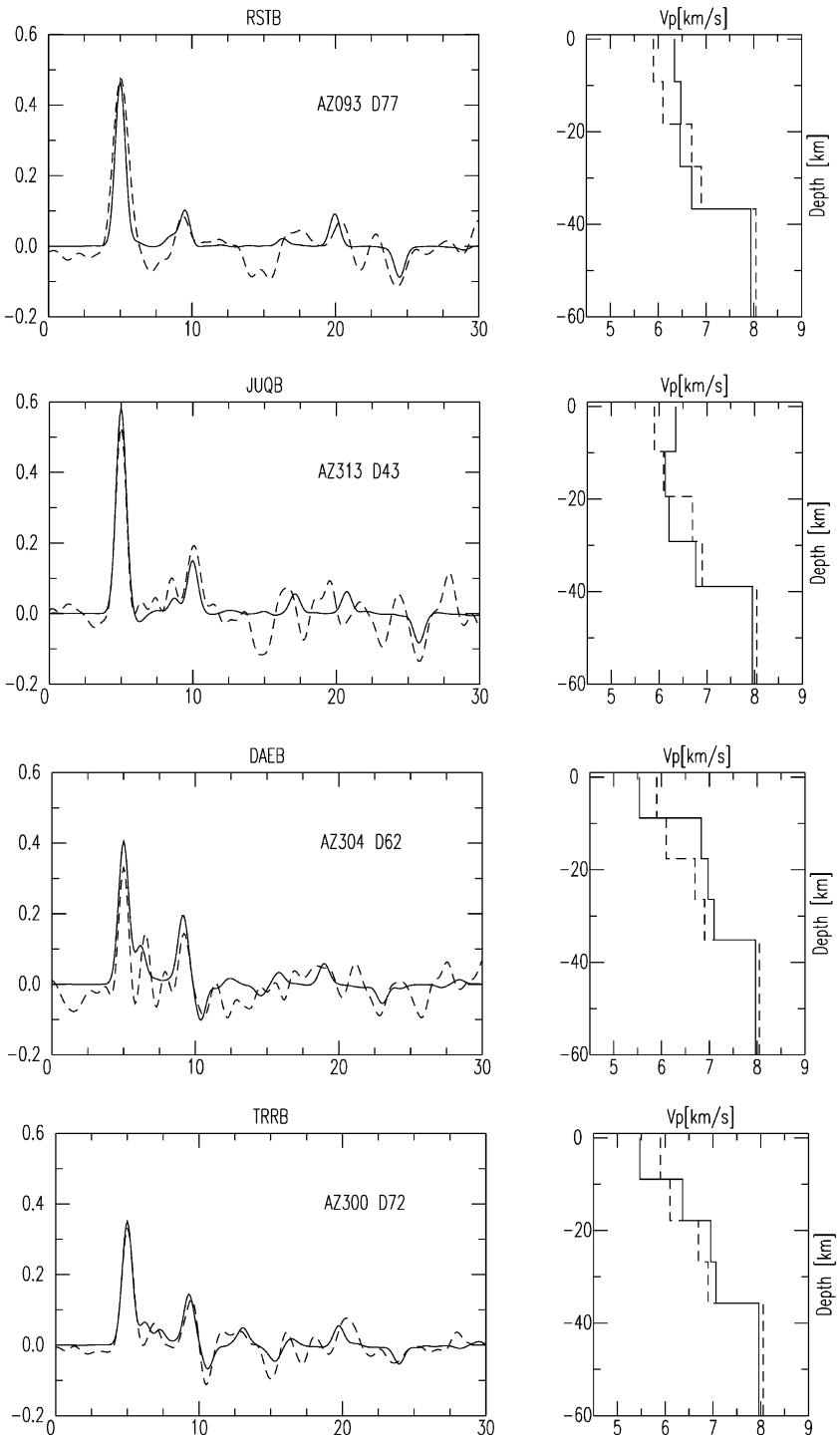

Fig. 17. Examples of synthetic RF for Serra do Mar stations. Left-hand column shows the observed trace (dashed line) and the inverted RF (solid line). Right-hand column shows the initial velocity model (dashed line) and inverted model (solid line).

Although, large variations are found within each province, the average elevation and crustal thickness values are roughly consistent with the Airy isostasy, as shown in Fig. 15 and in contrast with the relation between the center part of Paraná basin (low altitude and thicker crust) and the São Francisco craton (relatively higher altitude and thinner crust), which does not follow Airy isostasy (Assumpção et al., 2002). A significant difference in the average lithospheric composition between the basin and the craton may account for the Pratt type of isostasy. Alternatively, the average crustal density might not vary as much within the same geological province, such as the Ribeira belt, as

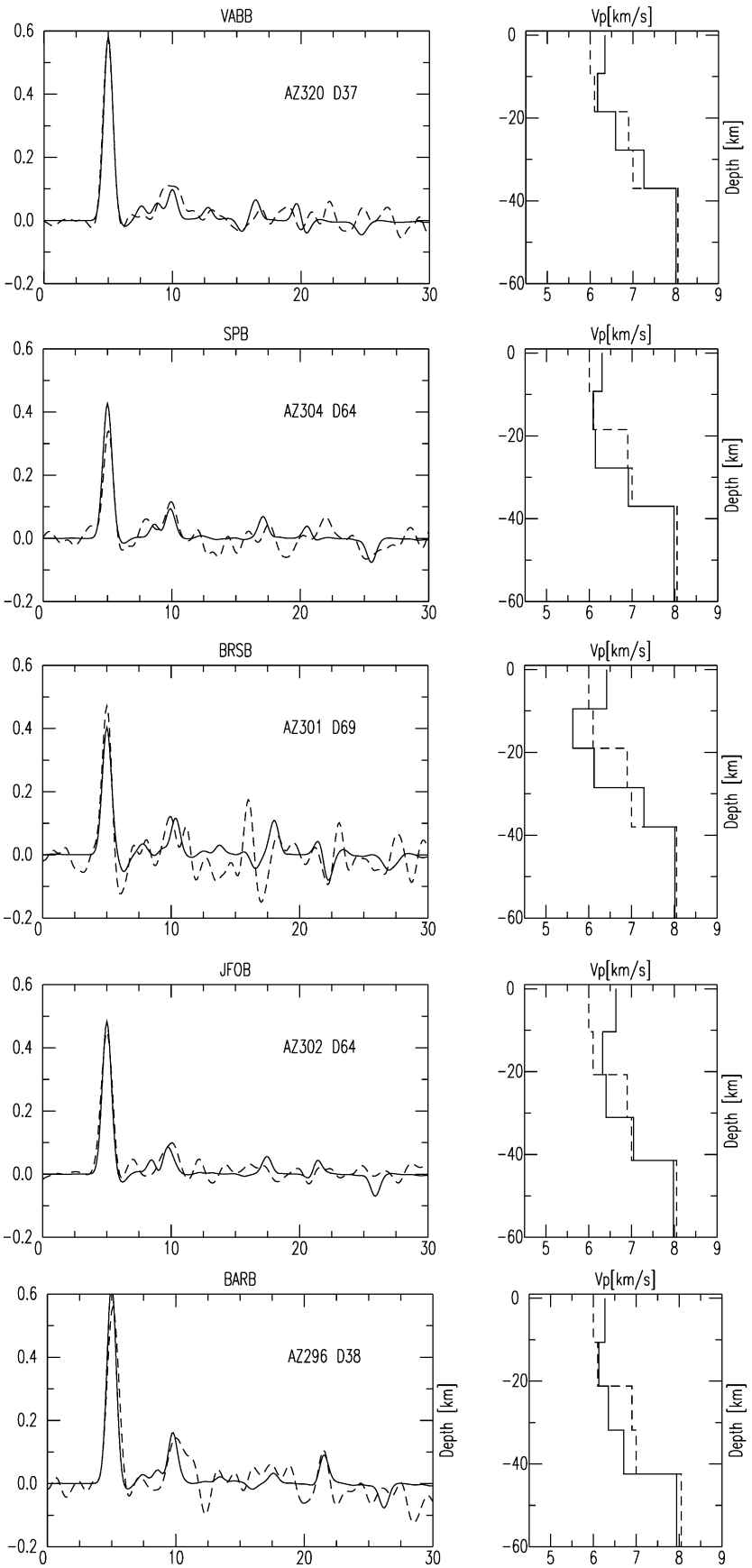

Fig. 18. Examples of synthetic RF for Mantiqueira stations. Legend and symbols as in Fig. 17.

between two different provinces. The large variation in altitudes helps demonstrate the Airy component of isostasy in the Ribeira belt.

Within the Ribeira belt, small departures from the Airy relation of Fig. 15 can be explained in various ways. For example, the PARB, IGAB, and DAEB stations, which are near the Itapeti quarry (Fig. 1b), have altitudes a few hundred meters higher than expected from their Bouguer anomaly (−60 to −70 mGal) or their crustal thickness (34–35 km). This may be interpreted as due to a crustal density lower than the average for the Ribeira belt or, alternatively, as an uplifted area of the Serra do Mar maintained at high altitudes by flexural stresses from the rifting process of the Atlantic margin.

Another interesting observation is the 5 km difference in crustal thickness between two nearby stations, TRRB (36 km) and JFOB (41 km), which is the largest Moho gradient in our study region (Figs. 1b and 14). One possible explanation may be the different kind of faulting and deformation beneath each station. The thinner crust beneath TRRB is characterized by large transcurrent faults, whereas beneath JFOB, thrust faulting during the Brasiliano orogeny may have increased the crustal thickness (Fig. 1a).

In addition to new estimates of Moho depth in SE Brazil, we present the first results of average crustal v_P/v_S ratios, which can be related to average crustal composition and density. These results should be helpful for future studies of crustal structure and evolution in SE Brazil.

Acknowledgements

We thank José Roberto Barbosa (IAG) for his effort and responsibilities during fieldwork. The comments and reviews of Martin Schimmel are appreciated. We also thank Monica Heilbron and David James for comments that helped improve the paper. The RF code was kindly provided by Charles Ammon, and the PWS program was provided by Martin Schimmel. Maps were plotted using GMT (Wessel and Smith, 1991), and seismograms were analyzed with SAC (Goldstein et al., 2000). Eder Molina provided the gravity data.

References

Ammon, C.J., 1991. The isolation effects from teleseismic P-waveforms. Bull. Seism. Soc. Am. 81, 2504–2510.

Ammon, C.J., Randall, G.E., Zandt, G., 1990. On the nonuniqueness of receiver functions inversions. J. Geophys. Res. 95, 15303–15318.

Assumpção, M., James, D., Snoke, J.A., 2002. Crustal thicknesses in SE Brazilian shield with receiver function: implications for isostatic compensation. J. Geophys. Res. 107, 2–11.

Bassini, A.M., 1986. Levantamento sismográficos na região sudeste do Brasil. Dissertação de Mestrado, Instituto de Astromomia, Geofísica e Ciências Atmosféricas/USP, São Paulo, Brasil, 162 pp. (in portuguese).

Berteussen, K.A., 1977. Moho depth determinations based on spectral ratio analysis of NORSAR long-period P waves. Phys. Earth Planet. Int. 31, 313–326.

Christensen, N.I., 1996. Poisson's ratio and crustal seismology. J. Geophys. Res. 101, 3139–3156.

Christensen, N.I., Mooney, W.D., 1995. Seismic velocity structure and composition of the continental crust: a global view. J. Geophys. Res. 100, 9761–9788.

Clayton, R.W., Wiggins, R.A., 1976. Source shape estimation and deconvolution of telesseismic bodywave. Geophys. J. R. Astron. Soc. 47, 151–177.

Giese, P., Shutte, J., 1975. Preliminary Report on the Results of Seismic Measurements in the Brazilian Coastal Mountains in March/April 1975, Free University of Berlin, Germany, 12 pp.

Goldstein, P., Dodge, D., Firpo, M., 2000. 'SAC2000': Signal processing and analysis tools for seismologists and engineers, UCRL-JC-135963, in: IASPEI International Handbook of Earthquake and Engineering Seismology.

Heilbron, M., Machado, N., 2003. Timing of terrane accretion in the Neoproterozoic-Eopaleozoic Ribeira orogen. Precambrian Res. 125, 87–112.

Holbrook, W.S., Mooney, W.D., Christensen, N., 1992. The seismic velocity structure of the deep continental crust. In: Fountain, D.M., Arculus, R., Kay, R.W. (Eds.), Continental Lower Crust, Developments in Geotectonics, vol. 23. Elsevier, New York, pp. 1–34.

Kennett, B.L.N., 1983. Seismic Wave Propagation in Stratified Media, Cambridge, 342 pp.

Langston, C.A., 1977. The effect of planar dipping structure source and receiver responses for constant ray parameter. Bull. Seism. Soc. Am. 67, 1029–1050.

Langston, C.A., 1979. Structure under Mount Rainier, Washington, inferred from teleseismic body waves. J. Geophys. Res. 85, 4749–4762.

Levin, V., Park, J., 1997. Crustal anisotropy in the Ural Mountains foredeep from teleseismic receiver functions. Geophys. R. Lett. 24(11), 1283–1286.

McNamara, D.E., Owens, T.J., 1993. Azimuthal shear wave velocity anisotropy in the basin and range province using moho Ps converted phase. J. Geophys. Res. 98, 12003–12017.

Owens, T.J., Crosson, R.S., 1988. Shallow structure effects on broadband teleseismic P waveforms. Bull. Seism. Soc. Am. 78, 96–108.

Owens, T.J., Zandt, G., Taylor, S.R., 1984. Seismic evidence for an ancient rift beneath the Cumberland plateau, Tennessee: a detailed analysis of broadband teleseismic P waveforms. J. Geophys. Res. 89, 7783–7795.

Owens, T.J., Taylor, S.R., Zandt, G., 1987. Crustal structure at regional seismic test network stations determined from inversion of broadband teleseismic P waveforms. Bull. Seism. Soc. Am. 77, 631–662.

Peng, X., Humphreys, E.D., 1997. Moho dip and crustal anisotropy in northwestern Nevada from teleseismic receiver functions. Bull. Seism. Soc. Am. 87(3), 745–754.

Perosi, F.A., 2000. Refração sísmica profunda no setor Sudeste da Província Tocantins, Dissertação de Mestrado, Instituto de Astromomia, Geofísica e Ciências Atmosféricas/USP, São Paulo, Brasil, 115pp. (in portuguese).

Schimmel, M., Paulssen, H., 1997. Noise reduction and detection of weak, coherent signals through phase-weighted stacks. Geophys. J. Int. 130, 497–505.

Schobbenhaus, C., Bellizia, A., 2001. Geological map of South America, 1:5000000, CGMW-CPRM-DPNM-UNESCO, Brasília-DF-Brazil.

Soares, J.E.P., Berrocal, J., Antunes, J.A., 2001. The Cavalcante and Miruau-Brasília deep seismic refraction lines: A travel time interpretation of crustal structure in central Brazil, Seventh International Congress of the Brazilian Geophysical Society, pp. 1341–1344.

Trompette, R., 2000. Geology of western Gondwana (2000–500 Ma), in: Pan-African Brasiliano Aggregation South America and Africa, A.A. Balkema, Rotterdam and Brookfield, p. 345.

Trouw, R., Heilbron, M., Ribeiro, A., Paciullo, F., Valeraino, C.M., Almeida, J.C.H., Tupinambà, M., Andreis, R.R., 2000. The central segment of the Ribeira Belt. In: Cordani, U.G., Milani, E.J., Thomaz Filho, A., Campos, D.A. (Eds.), Tectonic Evolution of South America, 31st International Geological Congress, Rio de Janeiro, Brazil, pp. 287–310.

Vauchez, A., Tommasi, A., Silva, M.E., 1994. Self-identation of a heterogeneous continental lithosphere. Geology 22, 967–970.

Wessel, P., Smith, W.H.F., 1991. Free software helps maps and displays data. Eos Trans. AGU 72(441), 445–446.

Zandt, G.S., Ammon, C.J., 1995. Continental crust composition constrained by measurements of crustal Poisson's ratio. Nature 374, 152–154.

Zandt, G.S., Myers, S.C., Wallace, T.C., 1995. Crust and mantle structure across the Basin and Range-Colorado Plateau boundary at 37° latitude and implications for Cenozoic extensional mechanism. J. Geophys. Res. 100(B6), 10529–10548.

Zhang, J.A., Langston, C.A., 1995. Dipping structure under Dourbes, Belgium, determined by receiver function modeling and inversion. Bull. Seism. Soc. Am. 85(1), 254–268.